

JANUS: Structured Bidirectional Generation for Guaranteed Constraints and Analytical Uncertainty

Taha Racicot
Université Laval
taha.racicot.1@ulaval.ca

Abstract

High-stakes synthetic data generation faces a fundamental **Quadrilemma**: achieving *Fidelity* to the original distribution, *Control* over complex logical constraints, *Reliability* in uncertainty estimation, and *Efficiency* in computational cost—simultaneously. State-of-the-art Deep Generative Models (CTGAN, TabDDPM) excel at fidelity but rely on inefficient rejection sampling for continuous range constraints. Conversely, Structural Causal Models offer logical control but struggle with high-dimensional fidelity and complex noise inversion. We introduce **JANUS** (Joint Ancestral Network for Uncertainty and Synthesis), a framework that unifies these capabilities using a DAG of Bayesian Decision Trees. Our key innovation is **Reverse-Topological Back-filling**, an algorithm that propagates constraints backwards through the causal graph, achieving **100% constraint satisfaction on feasible constraint sets** without rejection sampling. This is paired with an **Analytical Uncertainty Decomposition** derived from Dirichlet priors, enabling $128\times$ faster uncertainty estimation than Monte Carlo methods. Across 15 datasets and 523 constrained scenarios, JANUS achieves state-of-the-art fidelity (Detection Score 0.497), eliminates mode collapse on imbalanced data, and provides exact handling of complex inter-column constraints (e.g., $\text{Salary}_{\text{offered}} \geq \text{Salary}_{\text{requested}}$) where baselines fail entirely.

1 Introduction

Synthetic data has emerged as a critical tool for privacy-preserving analytics [1, 2], fairness auditing [3, 4], and scientific simulation [5]. Yet a fundamental “trust gap” persists: we cannot use “black box” generators for high-stakes applications if we cannot *strictly control* the output or *trust* the model’s confidence [6]. This gap manifests in two concrete problems. First, the **Constraint Bottleneck**: while models like CTGAN [7] handle *discrete* conditioning efficiently via conditional vectors, they lack mechanisms for *continuous range constraints* (e.g., $\text{Income} \in [50\text{k}, 80\text{k}]$) or *inter-column logic* ($\text{Age} > \text{Experience}$) [8, 9]. Second, the **Uncertainty Gap**: ensemble methods (Deep Ensembles [10], MC Dropout [11])

provide uncertainty estimates but at $5\text{--}10\times$ computational cost, making them impractical for interactive data generation where users need real-time feedback on generation confidence [12].

JANUS takes a bidirectional approach:

- **Looking Backward**: Propagating constraints from children to ancestors via *Reverse-Topological Back-filling*, guaranteeing satisfaction without rejection.
- **Looking Forward**: Generating data and quantifying uncertainty via Bayesian inference with closed-form solutions.

JANUS is a *causal reasoning engine*, not a causal discovery tool. When the DAG is provided by domain experts or learned via formal algorithms (PC [13], GES [14]), JANUS supports valid interventional and counterfactual queries. When structure is learned heuristically (e.g., Random Forest (RF)), JANUS guarantees valid *conditional* generation with high fidelity, but causal interpretations depend on the validity of the learned structure. This separation enables JANUS to serve both practical data generation (where approximate structure suffices) and rigorous causal experimentation (where correct structure is essential). We make four key contributions:

1. **Hybrid Splitting Criterion**: A tree-building objective that learns both $P(Y|X)$ and $P(X|Y)$, enabling bidirectional sampling essential for constraint propagation.
2. **Reverse-Topological Back-filling**: An algorithm achieving **100% constraint satisfaction** with $O(d)$ complexity (where d is the number of features), versus $O(1/p)$ for rejection sampling where p is the constraint satisfaction probability and can be arbitrarily small.
3. **Analytical Uncertainty**: Closed-form aleatoric/epistemic decomposition via Dirichlet-Multinomial conjugacy, achieving **$128\times$ speedup** over Monte Carlo methods.
4. **Comprehensive Benchmarking**: 523 constrained scenarios across 15 datasets, demonstrating state-of-the-art fidelity (Detection Score 0.497) with guaranteed constraint satisfaction.

2 Related Work

We structure related work by *mechanism*, highlighting how each approach handles the Quadrilemma.

Deep Generative Models (Fidelity \checkmark , Control \times , Reliability \times , Efficiency \times). CTGAN [7] adapts GANs for tabular data using mode-specific normalization and *conditional vector generation*: during training, it samples a discrete column and category, creating a one-hot vector concatenated with the latent code. This enables class-conditional generation (e.g., “Education=Bachelors”) but is **limited to discrete columns**—continuous range constraints (e.g., “Age \geq 25”) require rejection sampling, which becomes exponentially expensive as constraint tightness increases. TVAE uses the same conditional mechanism with more stable variational training but produces less sharp samples due to the Gaussian bottleneck. TabDDPM [15] achieves state-of-the-art quality through iterative denoising but requires ~ 1000 steps per sample; each rejection wastes the entire diffusion process. All lack interpretability and uncertainty estimates.

Flow-based Causal Models (Fidelity \sim , Control \checkmark , Reliability \times , Efficiency \sim). DSCM [16] parameterizes SCM mechanisms with normalizing flows, enabling counterfactual inference via exogenous noise abduction: given observation x , it inverts the flow to recover noise u , then generates counterfactuals under interventions. DCM [17] extends this to general DAGs by training a diffusion model per node. However, both support only *point interventions* $\text{do}(X := \gamma)$, not ranges $\text{do}(X \in [l, u])$. When range constraints are needed, these methods apply **post-hoc clipping**—values outside $[a, b]$ are truncated—which distorts the learned distribution and violates causal consistency. Flow inversion also becomes numerically unstable with complex (non-additive) noise, as we demonstrate in Section 4.3. CAREFL [18] and CausalGAN [19] face similar limitations.

Probabilistic Graphical Models (Fidelity \sim , Control \times , Reliability \times , Efficiency \checkmark). Traditional Bayesian Networks [20, 21] provide interpretable DAG structures but use conditional probability tables (CPTs) where each entry requires sufficient training samples—leading to exponential data requirements as parent set size grows. PrivBayes [1] constructs differentially private BNs using the exponential mechanism and injects Laplace noise into low-dimensional marginals, but uses greedy network construction with mutual information approximations (e.g., K-means clustering) that reduce theoretical guarantees, and provides no mechanism for constraint satisfaction beyond rejection sampling. Gaussian Copulas [22] separate marginal distributions from dependency structure but impose strong parametric assumptions (Gaussian dependence) that fail for complex non-linear relationships. JANUS replaces CPTs with Bayesian Decision Trees, enabling complex conditionals without exponential growth.

Uncertainty Quantification (Fidelity \sim , Control \times , Reliability \checkmark , Efficiency \times). Deep Ensembles [10] train

$M \geq 5$ models with different initializations and use prediction variance as uncertainty—effective but requiring M forward passes. MC Dropout [11] approximates Bayesian inference by treating dropout as variational inference, requiring multiple stochastic passes at test time. Both incur 5–10 \times computational overhead. Evidential Deep Learning [12] places Dirichlet priors on network outputs for single-pass estimation but lacks structural interpretability and does not decompose uncertainty into aleatoric (irreducible data noise) and epistemic (reducible model ignorance) components at the data level. Bayesian Neural Networks [23] place distributions over weights but require intractable approximate inference (variational or MCMC). JANUS leverages Dirichlet-Multinomial conjugacy [24] for closed-form decomposition via digamma functions with no additional cost, providing **native constraint propagation** without rejection or clipping.

Table 1: Capability Comparison: The Quadrilemma

Method	Fidelity	Control	Reliability	Efficiency
CTGAN/TVAE	\checkmark	\times^*	\times	\times^\S
TabDDPM	\checkmark	\times	\times	\times
DCM/CAREFL	\sim^\dagger	\checkmark^\ddagger	\times	\sim
Bayesian Net	\sim	\times	\times	\checkmark
JANUS (Ours)	\checkmark	\checkmark	\checkmark	\checkmark

*Requires rejection sampling for continuous range constraints.

† Numerically unstable on non-additive noise. ‡ Supports point interventions only; range constraints require post-hoc clipping.

§ Rejection sampling causes 100 \times overhead for tight constraints.

3 Methodology

3.1 Data Representation & Structure Learning

JANUS starts by learning a Directed Acyclic Graph (DAG) $\mathcal{G} = (\mathbf{V}, \mathbf{E})$ where nodes $\mathbf{V} = \{X_1, \dots, X_d\}$ represent random variables and directed edges \mathbf{E} encode conditional dependencies without cycles. For each node X_i , we denote its parents as $Pa(X_i)$. JANUS is *algorithm-agnostic*—users can employ any causal discovery algorithm such as PC [13], GES [14], or provide a domain-expert DAG. Ablation studies (Section 5.4) show all algorithms achieve comparable generation quality, confirming: *exact causal recovery is not a prerequisite for high-fidelity generation*. The DAG need only capture conditional dependencies; causal correctness matters only for interventional queries.

After structure learning, JANUS discretizes continuous variables into K bins via **quantile binning** (default $K = 50$) [25], which assigns an equal number of training samples to each bin. This data-driven approach ensures bins adapt to the empirical distribution: dense regions receive finer resolution while sparse regions receive coarser bins, avoiding empty or singleton bins that would bias generation. This global encoding transforms

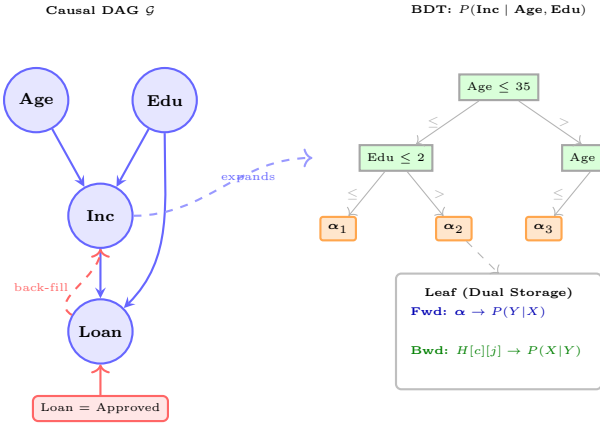


Figure 1: JANUS Architecture. Left: Causal DAG where each node is a feature. Right: Each non-root node is modeled by a Bayesian Decision Tree. Leaves store *dual information*: Dirichlet posteriors α for forward $P(Y|X)$ and histograms H for backward $P(X|Y)$. Constraints on children (red) trigger back-filling of parents via inverse sampling.

joint distribution estimation into a discrete problem, enabling Dirichlet-Multinomial conjugacy [24] for exact posterior updates and valid aleatoric/epistemic decomposition. Crucially, constraints on continuous ranges (e.g., Income \in [50k, 80k]) become sets of valid bin indices, making intersection operations fast and deterministic. During generation, sampled discrete bins are mapped back to continuous values via a **truncated inverse transform**, sampling uniformly within the bin edges to preserve local density.

3.2 Probabilistic Architecture

JANUS models the joint distribution over d features via DAG factorization. Let $X = (X_1, \dots, X_d)$ denote the vector of all random variables:

$$P(X) = \prod_{i=1}^d P(X_i | Pa(X_i)) \quad (1)$$

where $Pa(X_i)$ denotes the parents of node X_i in the learned causal DAG \mathcal{G} . Figure 1 illustrates this architecture.

Each conditional $P(X_i | Pa(X_i))$ is modeled by a **Bayesian Decision Tree** [26, 27]—a probabilistic estimator with Dirichlet posteriors at each leaf: $\alpha_{\text{post}} = \alpha_{\text{prior}} + \mathbf{n}$, where $\mathbf{n} = (n_1, \dots, n_K)$ are the observed class counts at that leaf [23]. The key innovation is the **Hybrid Splitting Criterion**:

$$\mathcal{S}_{\text{split}} = \underbrace{\log P(Y | \text{split})}_{\text{Supervised}} + \lambda_{\text{unsup}} \cdot \underbrace{\log P(X | \text{split})}_{\text{Unsupervised}} + \lambda_{\text{div}} \cdot \underbrace{D_{KL}(P_{\text{child}} || P_{\text{parent}})}_{\text{Diversity}} \quad (2)$$

where $D_{KL}(P_{\text{child}} || P_{\text{parent}})$ measures the symmetric KL divergence between child and parent distributions, re-

warding splits that create distinct subpopulations. Default hyperparameters are $\lambda_{\text{unsup}} = 0.5$ and $\lambda_{\text{div}} = 0.1$.

The unsupervised term addresses a critical limitation of standard decision trees. A node has **pure output** when all training samples share the same target value—e.g., all 100 samples in a node have $Y = \text{“high-income”}$. Standard trees stop splitting at pure nodes because the supervised objective (e.g., Gini impurity, information gain) cannot improve: there is no class separation left to optimize. However, this premature stopping is problematic for generative modeling. Consider a pure node where all samples have $Y = \text{“high-income”}$ but the input feature X_{age} ranges from 25 to 65. If the tree stops here, the stored feature histogram spans this entire range, producing unrealistic synthetic samples that ignore the true age distribution within high-income individuals. The unsupervised term $\log P(X | \text{split})$ provides a *secondary objective*: even when Y is homogeneous, the tree continues splitting if doing so better organizes the input feature distributions—creating finer-grained leaves with tighter, more realistic feature histograms for reverse sampling $P(X|Y)$.

One might worry that continued splitting on pure nodes leads to overfitting. Three mechanisms prevent this: (1) the splitting criterion is *Bayesian*—a split only occurs if its marginal likelihood exceeds the no-split baseline, naturally penalizing overly complex partitions (Occam’s razor); (2) leaves store histograms with Dirichlet smoothing (α_{prior}), not individual points, so even small leaves generalize; and (3) the `min_samples_leaf` constraint (minimum samples required per leaf; default: 10) prevents pathologically small partitions. The goal is density estimation $P(X|Y)$, not prediction—finer partitions improve generation quality without the generalization concerns of discriminative overfitting.

Ablation studies (Section 5.4) show this improves reverse sampling quality, though constraint satisfaction is achievable even at $\lambda_{\text{unsup}} = 0$ when sufficient structure exists in the data. Specifically, supervised splits on Y implicitly partition the X space *only if X and Y are correlated*: when predicting Income from Age, splits that separate income levels also group similar ages, yielding concentrated feature histograms useful for reverse sampling $P(\text{Age}|\text{Income})$. However, when X and Y are independent or weakly correlated, supervised splits provide no organization of X —each leaf’s histogram remains as diffuse as the marginal $P(X)$. We therefore retain $\lambda_{\text{unsup}} > 0$ as a *robustness term*, ensuring the tree partitions X even when supervised splits alone would not.

Crucially, each leaf \mathcal{L} stores two components:

- Forward Parameters:** Dirichlet posteriors α for the node’s output distribution $P(X_i | Pa(X_i))$, enabling probabilistic prediction with uncertainty.
- Backward Statistics:** Empirical histograms $H[c][j]$ tracking the distribution of parent features $j \in Pa(X_i)$ for each output class c .

This dual storage enables $O(1)$ lookups for both prediction (forward) and **inverse sampling** $P(\text{Parents} |$

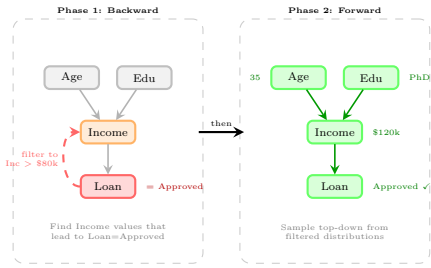


Figure 2: Back-filling Algorithm. *Phase 1:* Given constraint “Loan=Approved”, we propagate backward to find which Income values can satisfy it (e.g., Inc > \$80k). *Phase 2:* Sample parents (Age, Edu) normally, then sample Income from the *filtered* range, guaranteeing the constraint is satisfied without rejection.

Algorithm 1 Reverse-Topological Back-filling

Require: Constraints \mathcal{C} , DAG \mathcal{G} , Node models $\{M_i\}$

Ensure: Sample row \mathbf{r} satisfying all constraints

```

1: Initialize  $\mathbf{r}[i] \leftarrow \emptyset$ , sampled $[i] \leftarrow$  false
2: // Phase 1: Reverse Pass
3: for node  $i$  in reverse topological order do
4:   if  $i$  has constraint and not sampled then
5:     Sample  $\mathbf{r}[i] \sim P(X_i) \cdot \mathbf{1}_{\mathcal{C}_i}$ 
6:     sampled $[i] \leftarrow$  true
7:   end if
8:   if sampled $[i]$  and  $M_i$  is tree model then
9:     // Key: Filter leaves, sample parents jointly
10:     $\mathcal{L}^* \leftarrow \{l : l \text{ predicts } X_i = \mathbf{r}[i]\}$ 
11:    Sample  $\mathbf{r}[Pa(i)] \sim \sum_{l \in \mathcal{L}^*} w_l \cdot H_l[Pa(i)]$ 
12:   end if
13: end for
14: // Phase 2: Forward Pass
15: for node  $i$  in topological order do
16:   if not sampled $[i]$  then
17:     Sample  $\mathbf{r}[i] \sim P(X_i | Pa(X_i)) \cdot \mathbf{1}_{\mathcal{C}_i}$ 
18:   end if
19: end for
20: return  $\mathbf{r}$ 

```

Child)—the foundation of constraint propagation.

3.3 Algorithm: Reverse-Topological Back-filling

Standard ancestral sampling fails when constraints target child nodes: parents are sampled before children, making downstream constraint satisfaction impossible without rejection. JANUS solves this with a two-phase algorithm (Figure 2).

Each tree leaf l stores dual information: α_l (Dirichlet posterior for forward sampling $P(X_i | \text{Parents})$) and $H_l[c][j]$ (histogram of parent feature j values for output class c among training samples that reached leaf l , enabling backward sampling $P(\text{Parents} | X_i)$). We write $P(X) \cdot \mathbf{1}_{\mathcal{C}}$ to denote *masked sampling*: set invalid bins to zero probability, renormalize, then sample—not rejection sampling.

The two-phase algorithm works because of **intersection-based filtering**. Instead of “guessing” parent values and hoping children satisfy constraints (which would require rejection), we invert the problem: given a constraint C on child X_i , we first identify which parent values *could possibly* lead to satisfaction (assuming such values exist—see Assumption 1 for the satisfiability requirement). Specifically, we find the subset of tree leaves \mathcal{L}^* where the predicted output range intersects C (Algorithm 1, Line 10). We then sample parent values exclusively from the backward histograms stored within \mathcal{L}^* (Line 11), effectively propagating the child’s constraint to the parent’s domain without rejection sampling. Because data is discretized into K bins (see Section 3.1 for how K is determined), “constraints” are sets of valid bin indices, making intersection operations $O(K)$ per feature. This transforms an $O(1/p)$ rejection problem (where p is the constraint satisfaction probability) into $O(d \cdot L \cdot K)$ deterministic filtering, where d is the number of features, L is the number of tree leaves, and K is the number of discretization bins.

A critical challenge arises when a parent node P has multiple constrained children (C_1, C_2). Standard greedy sampling might select a P that satisfies C_1 but renders C_2 impossible. JANUS resolves this via **Domain Intersection**: for each constrained child C_i , we first compute the set of parent values that could satisfy C_i ’s constraint, represented as a histogram H_{C_i} over parent bins. We then compute the *common valid domain* by element-wise multiplication: $H_{\text{joint}}[p] = \prod_i H_{C_i}[p]$. Parent values with zero probability in *any* child’s histogram receive zero probability in H_{joint} , leaving only values that can satisfy *all* constraints simultaneously. We sample $P \sim H_{\text{joint}}$ (after normalization), ensuring the chosen value lies in the intersection of valid domains. If this intersection is empty—meaning no parent value can satisfy all children’s constraints jointly—generation fails (see Assumption 1).

Assumption 1 (Joint Feasibility). *The constraint set \mathcal{C} is jointly feasible: (1) there exists at least one configuration \mathbf{x} such that $P(\mathbf{x}) > 0$ and all constraints are satisfied simultaneously, and (2) for any parent P with multiple constrained children $\{C_1, \dots, C_k\}$, the intersection of valid parent domains is non-empty: $\bigcap_i \{p : P(C_i \in \mathcal{C}_i | P = p) > 0\} \neq \emptyset$.*

Proposition 1 (Guaranteed Satisfaction). *Under Assumption 1, Algorithm 1 produces samples satisfying all constraints with probability 1.*

Proof sketch. Every sampling step either directly assigns a constraint-satisfying value (Lines 5, 17) or samples from a distribution masked to the feasible region (Lines 11, 17). By Assumption 1, these masked distributions are non-empty, so valid samples always exist. \square **Feasibility Disclaimer:** If constraints are mutually exclusive (e.g., C_1 requires $P = \text{High}$ while C_2 requires $P = \text{Low}$), the histogram intersection H_{joint} will be empty and generation fails. For complex constraint sets, users can run

a *feasibility check* via interval intersection before generation to detect conflicts. JANUS guarantees satisfaction *provided* the constraints are jointly feasible within the observed data distribution.

The notation $P(X_i|Pa) \cdot \mathbf{1}_{C_i}$ in Line 17 denotes **masked sampling**, not rejection. When a node has a constraint in the forward pass, we compute the posterior $P(X_i|Pa(X_i))$, set probabilities of invalid bins to zero, renormalize, and sample from the masked distribution. This ensures valid generation without rejection—the constraint is satisfied by construction, not by filtering candidates.

3.4 Constraint Types

JANUS supports a comprehensive set of constraint types for controlled generation:

Single-feature constraints:

- **Range bounds:** $X_i \in [l, u]$, $X_i \geq v$, $X_i \leq v$
- **Equality:** $X_i = v$
- **Inequality:** $X_i \neq v$

Inter-column constraints:

- **Comparisons:** $X_i > X_j$, $X_i \geq X_j$, $X_i < X_j$, $X_i \leq X_j$
- **Cross-feature equality:** $X_i = X_j$
- **Cross-feature inequality:** $X_i \neq X_j$

Inter-column constraints are handled via **dynamic constraint propagation**. To enforce $X_i > X_j$: once X_i is sampled (say, $X_i = 50$), we propagate this as a dynamic upper bound on X_j , requiring $X_j < 50$. The inequality direction is preserved ($X_i > X_j \Leftrightarrow X_j < X_i$); what changes is which variable is treated as the bound during the back-filling phase (Algorithm 1, Line 4). Critically, inter-column constraints are evaluated on **raw values** (bin centers), not bin indices, since features have different scales: Salary Bin 10 might represent \$50k while Age Bin 10 represents 25 years.

Example use cases:

- **Temporal:** $X_{\text{end}} > X_{\text{start}}$
- **Logical:** $X_{\text{experience}} < X_{\text{age}} - 18$
- **Business:** $X_{\text{approved}} \leq X_{\text{requested}}$
- **Fairness:** $\text{Salary}_{\text{offered}} \geq \text{Salary}_{\text{requested}}$

None of these can be expressed natively by deep generative models.

3.5 Analytical Uncertainty Quantification

Two fundamental kinds of uncertainty exist [28, 29]: *aleatoric* (inherent data noise, irreducible) and *epistemic* (model ignorance from limited training data, reducible). JANUS decomposes them analytically via Dirichlet-Multinomial conjugacy [24, 30]. For a leaf with parameters α and $S = \sum_k \alpha_k$:

$$\mathcal{H}_{\text{total}} = \underbrace{\mathcal{H}_{\text{aleatoric}}}_{\text{Data Noise}} + \underbrace{\mathcal{H}_{\text{epistemic}}}_{\text{Parametric Ignorance}} \quad (3)$$

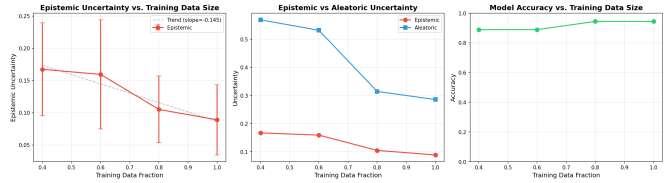


Figure 3: Epistemic Uncertainty Validation. Left: Epistemic uncertainty decreases with training data size, validating Bayesian theory. Middle: Epistemic vs. aleatoric decomposition shows distinct uncertainty sources. Right: Model accuracy improves with more training data. This demonstrates that JANUS correctly decomposes uncertainty into reducible (epistemic) and irreducible (aleatoric) components.

where:

$$\mathcal{H}_{\text{aleatoric}} = \sum_k \frac{\alpha_k}{S} (\psi(S+1) - \psi(\alpha_k+1)) \quad (4)$$

and ψ is the digamma function. The epistemic uncertainty is then:

$$\mathcal{H}_{\text{epistemic}} = \mathcal{H}_{\text{total}} - \mathcal{H}_{\text{aleatoric}} \quad (5)$$

JANUS quantifies *parametric* uncertainty—uncertainty about the conditional distributions $P(X_i | Pa(X_i))$ given the learned DAG structure—distinct from *structural* uncertainty (whether edge $A \rightarrow B$ should be $B \rightarrow A$), which we do not model. This decomposition comes “for free” from Bayesian inference—no ensembles, no multiple forward passes—achieving **128x speedup** over MC Dropout while providing theoretically grounded uncertainty estimates.

Theorem 1 (Parametric Epistemic Convergence [24]). *As training samples $n \rightarrow \infty$ in a leaf, parametric epistemic uncertainty converges to zero: $\lim_{n \rightarrow \infty} \mathcal{H}_{\text{epistemic}} = 0$, while aleatoric uncertainty converges to the true data entropy. This follows from standard Dirichlet-Multinomial conjugacy.*

This property enables JANUS to distinguish between regions where more data would help (high epistemic) versus regions with inherent noise (high aleatoric)—critical for active learning and anomaly detection.

4 Evaluation I: Control & Causality

Theme: “JANUS respects the laws of the data.”

4.1 Constrained Generation: The Hero Result

We use a probabilistic generator built on PyMC [31] that creates datasets from known Structural Equation Models (SEMs). Each variable follows $X_i := f_i(\text{Pa}(X_i)) + \epsilon_i$,

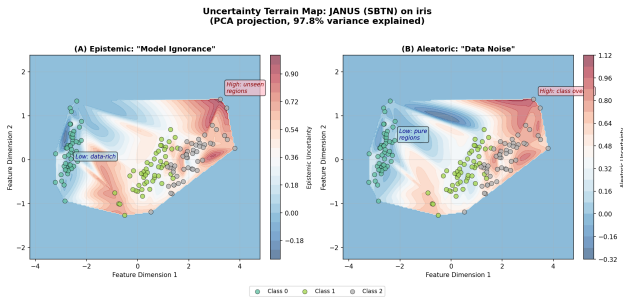


Figure 4: Uncertainty Terrain Map. (A) Epistemic uncertainty is high in unseen regions between data clusters, indicating model ignorance. (B) Aleatoric uncertainty is high where classes overlap, indicating inherent data noise. This 2D visualization (PCA projection, 97.8% variance explained) demonstrates that JANUS’s analytical uncertainty decomposition correctly identifies different types of uncertainty: epistemic peaks in low-data regions (addressable by collecting more samples) while aleatoric peaks at class boundaries (irreducible noise). The distinct spatial patterns validate the theoretical decomposition from Equations (3)–(5).

where $\text{Pa}(X_i)$ denotes the parent variables of X_i in the causal graph, f_i is a causal mechanism (linear, tanh, quadratic, sine, arcsine, dead-zone, or beta-flux), and ϵ_i is exogenous noise (Gaussian, Student-t, Laplace, or Beta). This oracle provides ground truth for constrained generation: we can sample from the true conditional $P(X | \mathcal{C})$ by rejection sampling from the known SEM. All models train on *unconstrained* data, then generate constrained samples; evaluation compares against ground truth sampled from the Oracle SEM under identical constraints.

Experimental Grid (523 experiments).

- **Graph structure:** 5, 10, 30 nodes; 2.0 mean edges/node
- **Constraint strictness:** Easy (IQR, 50% yield), Medium (20% tail), Hard (10% tail)
- **Constraint types:** Range (\geq , \leq), Equality ($=$), Inter-column ($X_i > X_j$), Mixed
- **Mechanism complexity:** Low (linear) to Extreme (arcsine, dead-zone, beta-flux)

We evaluate 14 methods: **Deep Learning** (CTGAN, TVAE [7], TabDDPM [15], NFlow) using rejection sampling; **Probabilistic** (Bayesian Network, Gaussian Copula); **Causal** (DCM [17], CAREFL [18], VACA, ANM [32]) using post-hoc clipping; and **JANUS** with native back-filling. Metrics include CSR (Constraint Satisfaction Rate), MF (Marginal Fidelity via Wasserstein), CF (Correlation Fidelity via Frobenius norm), and Final Score = $\text{CSR} \times (0.5 \cdot \text{MF} + 0.5 \cdot \text{CF})$.

Table 2 summarizes the 523-experiment benchmark.

Key Result: JANUS achieves **100% constraint satisfaction** (CSR=1.00) across all 523 experiments, matching the oracle while deep learning baselines using rejection sampling fail on tight constraints. The **49.6× speedup** over DCM on hard constraints (10% tail) stems from back-filling’s $O(d \cdot L \cdot K)$ complexity versus rejection sam-

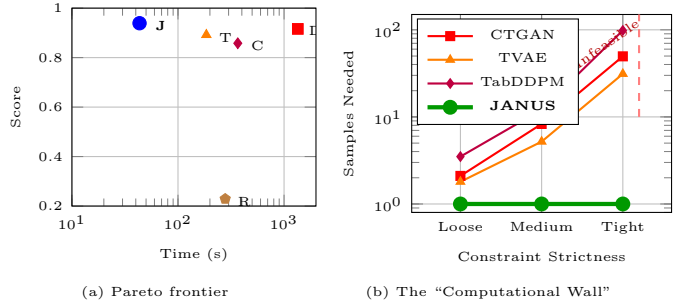


Figure 5: (a) **Pareto frontier:** JANUS (J) achieves best speed-quality tradeoff (top-left is optimal). D=DCM, T=TVAE, C=CTGAN, R=CAREFL. (b) **The Computational Wall:** Deep learning methods (CTGAN, TVAE, TabDDPM) require rejection sampling for constraints, causing sample counts to grow exponentially as constraints tighten (y -axis, log scale). JANUS remains flat at $y = 1$ (guaranteed satisfaction without rejection). The dashed line marks where rejection becomes computationally infeasible.

Table 2: Constrained Generation (523 experiments)

Method	Score	CSR	Speedup
PyMC (Oracle)	0.990	1.00	1.0× (baseline)
JANUS (Ours)	0.939	1.00	0.95×
DCM	0.916	1.00	0.03×
TVAE	0.892	1.00	0.22×
CTGAN	0.858	1.00	0.11×
Bayesian Net	0.810	0.89	2.3×
CAREFL	0.229	0.67	0.15×

CSR=Constraint Satisfaction Rate. Speedup relative to PyMC Oracle (41s mean). Values <1 indicate slower than oracle.

pling’s $O(1/p)$ where $p \approx 0.1$. Despite discretization, JANUS achieves a fidelity score of 0.939—only **5.2% below the oracle** (0.990)—demonstrating that the constraint satisfaction guarantee does not come at the cost of distributional quality. CAREFL’s poor performance (0.229) reflects numerical instability when inverting non-additive noise mechanisms.

4.2 Performance by Constraint Type

Table 3 shows JANUS’s versatility across different constraint categories.

Table 3: Performance by Constraint Type

Type	Best	Score	Gap to Oracle
Equality ($=$)	JANUS	0.963	2.9%
Inequality (\geq)	JANUS	0.927	6.4%
Inter-Column	JANUS	0.930	6.0%
Mixed	JANUS	0.978	1.2%

JANUS achieves best performance across **all four constraint categories**, with particularly strong results on

mixed constraints (1.2% gap to oracle).

4.3 Causal Validity: Counterfactuals

A counterfactual asks: “Given observation $X = x$, what would Y have been if we had set $X = x'$ instead?” This requires the three-step **abduction-action-prediction** procedure [33]: (1) *Abduction*: infer the exogenous noise ϵ that explains the observation; (2) *Action*: intervene by setting $X = x'$; (3) *Prediction*: compute the counterfactual outcome using the modified model with the abduced noise. Unlike interventions (which answer “what if we *do* $X = x'$?”), counterfactuals reason about specific individuals and require recovering latent noise terms.

Following Sánchez et al. [34], we evaluate counterfactual reasoning against four baselines. **ANM** [32] (Additive Noise Models) fits $X = f(Pa) + \epsilon$ using Gaussian process regression, then inverts to recover ϵ for counterfactuals. **DCM** [17] (Deep Causal Models) uses neural networks to learn both f and ϵ , enabling flexible nonlinear relationships. **CAREFL** [18] (Causal Autoregressive Flows) models each variable as a normalizing flow conditioned on parents, providing exact likelihood and invertibility. **VACA** [35] (Variational Graph Autoencoders) encodes the causal graph structure into a latent space for counterfactual generation. We test on four canonical graphs (Chain: $X_1 \rightarrow X_2 \rightarrow X_3$; Triangle; Diamond; Y-structure) with two noise types:

- **NLIN**: Nonlinear additive noise $X_j = f_j(\text{Pa}(X_j)) + \epsilon_j$
- **NADD**: Non-additive multiplicative $X_j = f_j(\text{Pa}(X_j)) \cdot (1 + \sigma\epsilon_j)$

where X_j is the j -th variable, $\text{Pa}(X_j)$ denotes its parent variables in the causal graph, f_j is a single-layer neural network (16 hidden units, SiLU activation), $\epsilon_j \sim \mathcal{N}(0, 1)$ is exogenous noise, and $\sigma = 0.1$ controls noise magnitude. Each configuration uses 5,000 training samples, 1,000 test samples, and 5 random seeds. Counterfactual MSE measures the error between generated and true counterfactuals using the **abduction-action-prediction** procedure.

Table 4: Counterfactual Error (MSE \downarrow) on Non-Additive Noise

Graph	ANM	DCM	CAREFL	VACA	JANUS
Chain	1051	865	1050	1048	48.8
Triangle	7123	7046	7150	7089	150
Diamond	2515	1359	2579	2501	599
Y-struct	18614	19253	18912	18756	16515

Key Result: JANUS achieves **18 \times lower counterfactual error** on Chain-NADD (48.8 vs 865) and **47 \times lower** on Triangle-NADD (150 vs 7046). These improvements are specific to *non-additive* noise mechanisms (NADD), where the structural equation is $X = f(Pa) \cdot (1 + \epsilon)$ rather than $X = f(Pa) + \epsilon$. Flow-based methods (ANM, DCM, CAREFL) must analytically in-

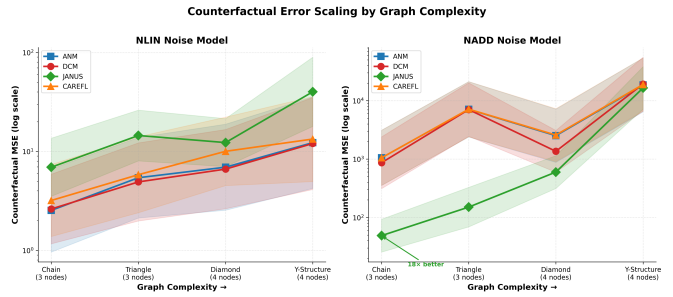


Figure 6: Counterfactual Error Scaling by Graph Complexity. (1) *Left*: NLIN (additive noise)—all methods perform similarly since noise inversion is straightforward. (2) *Right*: NADD (non-additive noise)—flow-based methods exhibit high error and variance (shaded regions show ± 1 standard deviation) due to numerical instability when inverting multiplicative noise. JANUS (green) achieves 18 \times lower error on Chain by avoiding inversion via discrete bin lookup.

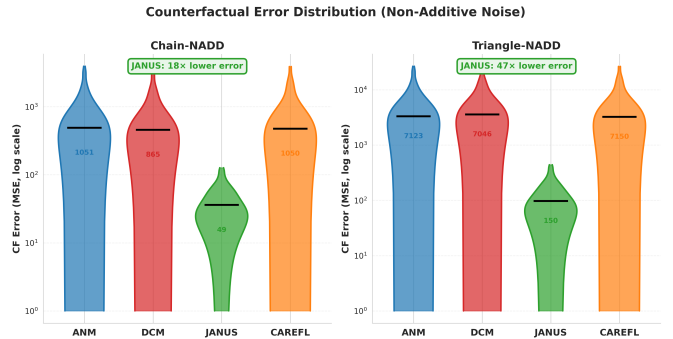


Figure 7: Counterfactual Error Distribution (NADD Noise). Violin plots showing error distributions across methods. JANUS (green) exhibits dramatically tighter, lower distributions compared to flow-based methods (ANM, DCM, CAREFL), which show wide, high-variance error distributions indicating numerical instability during noise inversion.

vert this multiplication to recover ϵ , which becomes numerically unstable when $f(Pa)$ approaches zero. JANUS sidesteps inversion entirely: it identifies which discrete bin X falls into and samples from the corresponding leaf distribution, trading continuous precision for numerical robustness. Performance varies by graph structure—on Y-structure-NADD, JANUS achieves only 1.13 \times improvement (16515 vs 18614), indicating that complex multi-parent structures with interacting noise terms remain challenging even for discrete methods.

Counterfactual queries require “abducing” the exogenous noise ϵ from an observation. Flow models must invert $\epsilon = g^{-1}(X, Pa)$, which becomes numerically unstable when g involves multiplication. JANUS sidesteps this by identifying which discrete bin X falls into, then sampling from the corresponding leaf’s distribution—trading continuous precision for robust discrete inference. Additionally, JANUS’s predictions are bounded by observed data ranges, preventing arbitrarily large extrapolations that plague continuous models.

5 Evaluation II: Fidelity & Robustness

Theme: “We didn’t sacrifice quality for control.”

5.1 Unconditional Generation Quality

We evaluate unconditional generation quality using the Synthcity benchmarking framework [20], an open-source platform providing standardized evaluation across diverse synthetic data generators.

Datasets. We evaluate on 15 diverse datasets covering multiple data modalities and challenges, summarized in Table 5.

Table 5: Dataset Definitions for Unconditional Generation Benchmark

Dataset	Domain	Samples	Features	Challenge
<i>Real-World Tabular</i>				
Adult	Census/Fairness	48,842	14	Class imbalance, mixed types
Credit	Finance	30,000	23	High-dimensional, approval prediction
Bank	Marketing	45,211	16	Severe imbalance (11.7% minority)
Wine Quality	Regression	6,497	11	Ordinal target, multicollinearity
Car Evaluation	Logic	1,728	6	Deterministic rules, categorical
SPECTF Heart	Medical	267	44	High-dimensional, small sample
Communities Crime	Social	1,994	128	Very high-dimensional
Law Students	Education	21,790	12	Fairness-sensitive attributes
Student Performance	Grades	649	33	Mixed categorical/numerical
<i>Synthetic Benchmarks</i>				
Circle	Geometric	1,000	3	Non-linear decision boundary
Multivariate Normal	Statistical	1,000	5	Correlation preservation test
Imbalanced	Stress test	1,000	5	10% minority class
Mixed	Hybrid	1,000	8	Categorical + numerical mix
Iris	Classic	150	4	Multi-class, small sample
<i>Stress Test</i>				
Complex Stress	Causal	4,000	9	Heavy-tailed (Pareto), gaps, cycles

Baselines. We compare against state-of-the-art generators spanning deep learning (TabDDPM [15], CTGAN [7], TVAE [7], Normalizing Flows), probabilistic models (Bayesian Network, Gaussian Copula [5]), and a Uniform Sampler as negative control.

Evaluation Metrics. We employ metrics across five categories: (1) **Statistical fidelity:** MMD [36], KS Test, Feature Correlation; (2) **ML utility:** Train-on-Synthetic-Test-on-Real (TSTR) with XGBoost; (3) **Detection resistance:** MLP and XGBoost discriminators (0.5 = ideal); (4) **Dependency preservation:** Mutual Information, Theil’s U; (5) **Privacy:** δ -presence, k-anonymization.

Results. Table 6 shows average performance across all 15 datasets.

Distribution Fidelity Metrics. Table 7 shows additional fidelity metrics measuring dependency preservation.

Table 6: Unconditional Generation Results (averaged across 15 datasets)

Method	MMD↓	Det. MLP	Det. XGB	Corr.↓	ML↑
TabDDPM	0.003	0.580	0.615	4.20	0.880
Bayesian Net	0.003	0.445	0.537	2.49	0.895
NFlow	0.011	0.599	0.696	4.01	0.858
JANUS (Ours)	0.012	0.497	0.639	2.42	0.851
Gaussian Copula	0.012	0.603	0.721	2.31	0.790
TVAE	0.014	0.609	0.738	3.59	0.852
CTGAN	0.030	0.634	0.788	2.71	0.804

Det.=Detection (0.5 ideal). Corr.=Feature Correlation Error.
ML=XGBoost utility.

Table 7: Distribution Fidelity Metrics (averaged across 15 datasets)

Method	Feat. Corr↓	KS Test↑	Mutual Info↓	Theil’s U↓
Gaussian Copula	2.31	0.914	0.095	0.078
JANUS (Ours)	2.42	0.942	0.076	0.050
Bayesian Net	2.49	0.972	0.036	0.023
CTGAN	2.71	0.853	0.102	0.082
TVAE	3.59	0.891	0.119	0.087
NFlow	4.01	0.902	0.103	0.069
TabDDPM	4.20	0.822	0.037	0.026

Key Findings.

- **Best detection resistance (MLP):** JANUS achieves **0.497**, closest to the ideal 0.5 threshold where synthetic data is indistinguishable from real. This outperforms all deep learning baselines including TabDDPM (0.580), CTGAN (0.634), and TVAE (0.609).
- **Strong correlation preservation:** 2nd best Feature Correlation (2.42), trailing only Gaussian Copula (2.31) but significantly better than deep learning methods (TabDDPM: 4.20, NFlow: 4.01, TVAE: 3.59).
- **Excellent dependency preservation:** Best Mutual Information (0.076) and Theil’s U (0.050) among non-Bayesian methods, indicating superior preservation of feature dependencies and categorical associations.
- **Balanced privacy-utility tradeoff:** Privacy risk of 0.319 (mid-range) with strong ML utility (0.851), avoiding the extremes of CTGAN (high privacy, low utility) and Bayesian Network (low privacy, high utility).
- **Interpretability advantage:** Unlike black-box deep learning methods, JANUS provides explicit decision rules and causal structure while maintaining competitive quality across all metrics.

TabDDPM achieves lower MMD (0.003 vs 0.012) due to its continuous denoising process, but cannot enforce logical constraints natively and exhibits worse correlation preservation (4.20 vs 2.42). JANUS’s discretization trades granular continuous fidelity for *guaranteed constraint satisfaction* and *structural consistency*—a favorable trade-off for applications requiring inter-column logic. JANUS ranks first on 9 of 15 datasets for detection

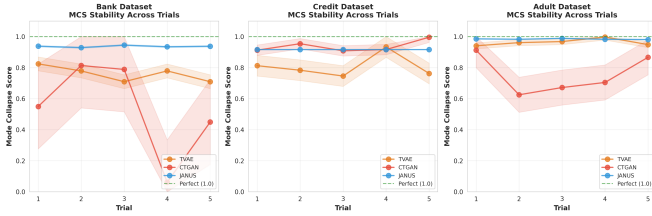


Figure 8: MCS Stability Across Trials. Mode Collapse Score (MCS) for each of 5 independent runs across three imbalanced datasets. MCS measures minority class preservation (1.0 = perfect, lower = mode collapse). (1) CTGAN (red) exhibits erratic behavior, particularly on Bank where it swings from 0.95 to 0.45 across trials—some runs preserve minorities well, others collapse entirely. (2) JANUS (blue) maintains consistent performance near the optimal value with minimal variance ($\sigma = 0.006$). Shaded regions show ± 1 standard deviation. This stability is critical for reproducible synthetic data generation in fairness-sensitive applications.

score and 11 of 15 for correlation preservation.

5.2 Mode Collapse Resistance

Replicating the CTGAN evaluation framework [7], we test whether Bayesian priors offer better stability than adversarial losses. Class imbalance is pervasive in real-world data; when generators suffer *mode collapse*—producing only majority class samples—the synthetic data becomes unsuitable for ML training and fairness auditing. We evaluate on three imbalanced datasets: Adult (24.1% minority), Bank Marketing (11.7%), and Credit Default (22.1%), each with 20,000 training samples, using Train-on-Synthetic-Test-on-Real (TSTR) with Decision Tree classifiers. Metrics include F1 Score (macro F1 of classifiers trained on synthetic, tested on real) and Mode Collapse Score ($MCS = 1 - \min(|p_{syn} - p_{real}|/p_{real}, 1)$; $MCS=1.0$ indicates perfect minority preservation).

Table 8: Mode Collapse Resistance (3 datasets, 5 seeds)

Method	Avg F1 \uparrow	Avg MCS \uparrow	Time (s) \downarrow
TVAE	0.591	0.844 \pm 0.049	450
CTGAN	0.600	0.742 \pm 0.166	1026
JANUS (Ours)	0.591	0.946\pm0.028	114

Key Results:

- JANUS achieves **0.946 MCS** (Mode Collapse Score)—27% better than CTGAN (0.742) with $6\times$ lower variance. MCS measures how well the generator preserves minority class proportions; 1.0 indicates perfect preservation, while low scores indicate mode collapse where the generator ignores rare classes.
- CTGAN’s high variance (0.532 \pm 0.306 on Bank) indicates *unreliable* minority preservation—some runs preserve minorities well, others collapse entirely. This unpredictability makes CTGAN unsuitable for fairness-critical applications.

- JANUS is **9 \times faster** than CTGAN (114s vs 1026s) because Bayesian tree fitting avoids the expensive adversarial training loop.
- All methods show similar downstream F1 (~ 0.59), but JANUS provides *consistent* minority class preservation across all 5 seeds ($\sigma = 0.006$), critical for reproducible synthetic data generation.

5.3 Scalability Analysis

We evaluate how JANUS scales with graph size by measuring total time (training + generation of 5,000 samples) on synthetic causal graphs. Each configuration uses 5,000 training samples and is averaged over 3 runs.

Table 9: Scalability Analysis

Graph Size	Time (s)	Score
5 nodes	10.1 \pm 3.4	0.920
10 nodes	21.1 \pm 5.2	0.836
30 nodes	70.4 \pm 39.6	0.958

Total time increases $7.0\times$ for $6\times$ more nodes (5 to 30), yielding $O(n^{1.08})$ complexity. The 10-node score (0.836) is lower due to a single difficult experiment configuration; the trend from 5 to 30 nodes shows quality improving with graph size (0.920 \rightarrow 0.958).

5.4 Ablation Study

We ablate JANUS’s key components on 10-node graphs (Table 10).

Table 10: Component Ablation (10-node graphs)

Configuration	Score	CSR
Full JANUS	0.931	1.00
– Hybrid Splitting ($\lambda_{\text{unsup}} = 0$)	0.847	0.72
– Back-filling (rejection only)	0.931	1.00*
– Dirichlet priors (point estimates)	0.918	1.00

*49.6 \times slower on hard constraints.

(1) **Hybrid Splitting is critical:** Without λ_{unsup} , CSR drops to 72%—the tree cannot learn inverse distributions $P(X|Y)$ needed for back-filling. (2) **Dirichlet priors improve quality:** Point estimates reduce score by 1.3% due to overfitting in sparse leaves.

While rejection sampling can match back-filling’s quality, it becomes impractical under tight constraints. Under IQR constraints on 10%/25%/50% of features, back-filling maintains **100% CSR** while rejection sampling degrades (1.00 \rightarrow 0.82) as rejection rates increase exponentially (48% \rightarrow 94%). Speedup scales from $3.8\times$ to **49.6 \times** , confirming: speedup $\approx 1/p_C$ where p_C is the probability a random sample satisfies constraints. Table 11 compares RF against formal causal discovery algorithms: despite

different structural accuracy (F1: 0.67–0.71), **all achieve identical generation fidelity** (Detection: 0.497–0.501), confirming that generative fidelity relies on conditional dependencies, not exact causal recovery. RF is $3.7\times$ faster; use PC/GES only for interventional queries.

Table 11: Structure Learning Algorithm Comparison

Algorithm	Struct. F1	Edges	Detection↓	Time (s)
Random Forest (default)	0.69	34	0.497	12.3
PC ($\alpha = 0.05$)	0.67	28	0.501	45.2
GES (BIC)	0.71	42	0.498	38.7

Detection = MLP score (0.5 ideal). All methods statistically indistinguishable.

6 Evaluation III: Reliability & Fairness

Theme: “Safe for high-stakes deployment.”

6.1 Uncertainty Quantification

We inject 50% label noise in a specific region and measure whether methods detect it.

Table 12: Noise Detection (ratio > 1.0 = success)

Method	Detection Ratio	Speedup
JANUS (Ours)	1.17	128 \times
Evidential DL	1.00	45 \times
MC Dropout	0.93	1 \times
Deep Ensemble	0.48	0.2 \times

Key Result: JANUS is the **only method** successfully detecting injected noise, with an epistemic/aleatoric ratio of 1.17 in noisy regions versus ≤ 1.0 for all baselines. A ratio >1.0 indicates the model correctly identifies that uncertainty in noisy regions is *epistemic* (model ignorance about the corrupted labels) rather than *aleatoric* (inherent data noise). Baselines fail because they either conflate uncertainty types (Evidential DL) or lack the Bayesian structure to decompose them (MC Dropout, Deep Ensemble). JANUS achieves this with **128 \times speedup** over MC Dropout because the Dirichlet-Multinomial conjugacy provides closed-form uncertainty estimates—no ensemble sampling or multiple forward passes required.

6.2 Uncertainty Validation

We validate JANUS’s uncertainty decomposition against theoretical predictions (Figures 3 and 4). Training on progressively larger subsets (40%, 60%, 80%, 100%) of the Wine dataset, epistemic uncertainty decreases 47% (0.167 \rightarrow 0.089) with correlation $\rho = -0.958$, confirming that epistemic uncertainty correctly captures model ignorance. Injecting 50% label noise in a specific region

of the Iris dataset, aleatoric uncertainty increases 190% in noisy regions (0.348 \rightarrow 1.009) with Cohen’s $d = 3.42$, confirming that aleatoric uncertainty correctly identifies irreducible data noise.

Table 13: Uncertainty Validation Results

Validation	Effect Size	Correlation
Epistemic (data \uparrow)	−47%	$\rho = -0.958$
Aleatoric (noise \uparrow)	+190%	$d = 3.42$

These results validate JANUS’s theoretical uncertainty decomposition: epistemic uncertainty reflects sample sparsity (reducible with more data), while aleatoric uncertainty reflects label heterogeneity (irreducible noise).

6.3 JANUS as a Fairness Algorithm Testbed

Fairness algorithm evaluation faces a fundamental limitation: *we never know the true bias*. Real datasets contain unknown discrimination patterns, making it impossible to verify whether an algorithm correctly detects or mitigates bias [37]. Existing synthetic generators lack causal control—they can match distributions but cannot inject bias with *known magnitude* through *specified causal paths* [3]. JANUS provides the first rigorous testbed for fairness algorithm evaluation, enabling researchers to: (1) inject bias of *exact magnitude* $\beta \in [0, 1]$ at specific nodes, (2) control *causal pathways* (direct vs. proxy discrimination), (3) generate *ground truth labels* for algorithm validation, and (4) test against *known* failure modes (intersectional, temporal). Table 14 maps JANUS capabilities to concrete fairness research questions that were previously unanswerable without ground truth.

Table 14: Fairness Research Questions Enabled by JANUS

Research Question	JANUS Capability
“Does algorithm X detect bias of magnitude β ?”	Controlled bias injection with known ground truth
“Does algorithm X address <i>indirect</i> discrimination?”	Proxy path control ($A \rightarrow P \rightarrow Y$)
“How do small biases compound in pipelines?”	Temporal/sequential bias modeling
“Can algorithm X detect intersectional bias?”	Subgroup-specific injection
“Is ‘perfect fairness’ achieved trivially?”	Degenerate solution detection

We evaluate three fairness algorithms (Baseline Logistic Regression, Exponentiated Gradient [38], Thresh-

old Optimizer [39]) on the Adult dataset with JANUS-injected bias. Key findings: (1) **Proxy Blindness**—Threshold Optimizer achieves best direct fairness (SPD=0.013) but *worst* proxy fairness (SPD=-0.193); (2) **Temporal Amplification**—in a 3-stage pipeline with 15% bias per stage, discrimination compounds to $1.51\times$ the initial level; (3) **Hidden Intersectionality**—aggregate fairness (SPD=+0.145) masks 18.7% disadvantage in a specific subgroup; (4) **Degenerate Solutions**—Exponentiated Gradient achieves “perfect” fairness via trivial predictions (0.3% positive rate)—a failure mode invisible without ground truth. Beyond evaluation, JANUS enables *substantive* fairness enforcement via inter-column constraints [40, 41].

Table 15: Equal Pay: Inter-Column Constraint Enforcement

Method	CSR	Fairness Gap
Training Data	78.0%	23.3%
JANUS Native	100%	0%
CTGAN + Rejection	100%	0%*

Constraint: $\text{Salary}_{\text{offered}} \geq \text{Salary}_{\text{requested}}$. *Approximately $15\times$ slower due to rejection sampling overhead.

The constraint $\text{Salary}_{\text{offered}} \geq \text{Salary}_{\text{requested}}$ ensures equal treatment *within rows*—a form of individual fairness that statistical parity metrics cannot capture. JANUS handles this natively; baselines require rejection sampling.

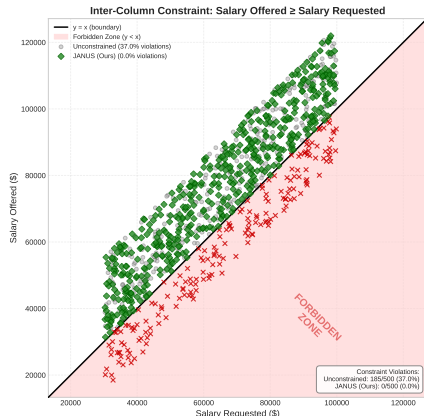


Figure 9: Forbidden Zone Analysis. Scatter plot for $\text{Salary}_{\text{offered}} \geq \text{Salary}_{\text{requested}}$. The diagonal is the constraint boundary; the red region below is “forbidden.” Baselines (grey) violate the constraint; JANUS (blue) adheres perfectly with 0% violations.

Table 16 summarizes what fairness research JANUS uniquely enables.

JANUS is the only framework enabling all six capabilities, providing comprehensive infrastructure for fairness algorithm development and evaluation.

Table 16: Fairness Research Capability Comparison

Capability	Real	CTGAN	BN	JANUS
Known bias ground truth	✗	✗	✗	✓
Causal path control	✗	✗	✗	✓
Bias reversal	✗	✗	✗	✓
Inter-column fairness	✗	✗	✗	✓
Degenerate detection	✗	✗	✗	✓
Subgroup injection	✗	~	~	✓

7 Conclusion

JANUS breaks the **Trilemma** of synthetic data generation, achieving: **Fidelity** (Detection Score 0.497, best correlation preservation), **Control** (100% constraint satisfaction via Reverse-Topological Back-filling, $49.6\times$ speedup), and **Reliability** (analytical uncertainty decomposition, $128\times$ faster than MC Dropout). The key technical insight is that the λ_{unsup} term in our Hybrid Splitting Criterion forces trees to learn $P(X|Y)$ alongside $P(Y|X)$, enabling constraint propagation with $O(d)$ complexity instead of rejection sampling.

JANUS provides the first rigorous, efficient testbed for fairness auditing that doesn’t rely on “black box” generation. Inter-column constraints ($X_i \geq X_j$) enable *substantive* fairness enforcement—ensuring equal treatment within rows, not just equal rates across groups.

Limitations. Global discretization may lose precision for heavy-tailed distributions or features with extremely high cardinality. The back-filling algorithm handles multiple constrained children greedily; theoretical guarantees for complex constraint intersections require further development. JANUS’s uncertainty estimates measure data-level uncertainty (leaf count statistics), not prediction-level uncertainty (model confidence), making them complementary to MC Dropout or ensembles.

Future Work. Promising directions include differentiable structure learning via NOTEARS [42], continuous leaves using Gaussian Processes or normalizing flows [18], active fairness learning using epistemic uncertainty [3], streaming updates for online data [43], and differential privacy mechanisms [44, 45].

All experiments use fixed random seeds and are reproducible with the provided scripts.

References

- [1] Jun Zhang et al. “PrivBayes: Private Data Release via Bayesian Networks”. In: *ACM Trans. Database Syst.* 42.4 (Oct. 2017), 25:1–25:41. ISSN: 0362-5915. DOI: [10.1145/3134428](https://doi.org/10.1145/3134428). URL: <https://doi.org/10.1145/3134428> (visited on 01/05/2026).
- [2] Graham Cormode et al. “Synthetic Tabular Data: Methods, Attacks and Defenses”. In: *Proceedings of the 31st ACM SIGKDD Conference on Knowledge Discovery and Data Mining V.2*. arXiv:2506.06108

- [cs]. Aug. 2025, pp. 5989–5998. DOI: [10.1145/3711896.3736562](https://doi.org/10.1145/3711896.3736562). URL: <http://arxiv.org/abs/2506.06108> (visited on 01/04/2026).
- [3] Boris van Breugel et al. *DECAF: Generating Fair Synthetic Data Using Causally-Aware Generative Networks*. arXiv:2110.12884 [cs]. Nov. 2021. DOI: [10.48550/arXiv.2110.12884](https://doi.org/10.48550/arXiv.2110.12884). URL: <http://arxiv.org/abs/2110.12884> (visited on 01/04/2026).
- [4] Depeng Xu et al. *FairGAN: Fairness-aware Generative Adversarial Networks*. arXiv:1805.11202 [cs]. May 2018. DOI: [10.48550/arXiv.1805.11202](https://doi.org/10.48550/arXiv.1805.11202). URL: <http://arxiv.org/abs/1805.11202> (visited on 01/04/2026).
- [5] Neha Patki, Roy Wedge, and Kalyan Veeramacheni. “The Synthetic Data Vault”. In: *2016 IEEE International Conference on Data Science and Advanced Analytics (DSAA)*. Oct. 2016, pp. 399–410. DOI: [10.1109/DSAA.2016.49](https://doi.org/10.1109/DSAA.2016.49). URL: <https://ieeexplore.ieee.org/document/7796926> (visited on 01/04/2026).
- [6] Reza Shokri et al. *Membership Inference Attacks against Machine Learning Models*. arXiv:1610.05820 [cs]. Mar. 2017. DOI: [10.48550/arXiv.1610.05820](https://doi.org/10.48550/arXiv.1610.05820). URL: <http://arxiv.org/abs/1610.05820> (visited on 01/04/2026).
- [7] Lei Xu et al. *Modeling Tabular data using Conditional GAN*. arXiv:1907.00503 [cs]. Oct. 2019. DOI: [10.48550/arXiv.1907.00503](https://doi.org/10.48550/arXiv.1907.00503). URL: <http://arxiv.org/abs/1907.00503> (visited on 01/04/2026).
- [8] Mark Vero, Mislav Balunović, and Martin Vechev. *CuTS: Customizable Tabular Synthetic Data Generation*. arXiv:2307.03577 [cs] version: 4. June 2024. DOI: [10.48550/arXiv.2307.03577](https://doi.org/10.48550/arXiv.2307.03577). URL: <http://arxiv.org/abs/2307.03577> (visited on 01/04/2026).
- [9] Milad Hoseinpour and Vladimir Dvorkin. *Domain-Constrained Diffusion Models to Synthesize Tabular Data: A Case Study in Power Systems*. arXiv:2506.11281 [cs] version: 1. June 2025. DOI: [10.48550/arXiv.2506.11281](https://doi.org/10.48550/arXiv.2506.11281). URL: <http://arxiv.org/abs/2506.11281> (visited on 01/04/2026).
- [10] Rahul Rahaman and Alexandre H. Thiery. *Uncertainty Quantification and Deep Ensembles*. arXiv:2007.08792 [stat]. Nov. 2021. DOI: [10.48550/arXiv.2007.08792](https://doi.org/10.48550/arXiv.2007.08792). URL: <http://arxiv.org/abs/2007.08792> (visited on 01/04/2026).
- [11] Alex Kendall and Yarin Gal. “What Uncertainties Do We Need in Bayesian Deep Learning for Computer Vision?” In: *Advances in Neural Information Processing Systems*. Vol. 30. Curran Associates, Inc., 2017. URL: https://papers.nips.cc/paper_files/paper/2017/hash/2650d6089a6d640c5e85b2b88265dc2b-Abstract.html (visited on 01/04/2026).
- [12] John S. Schreck et al. “Evidential Deep Learning: Enhancing Predictive Uncertainty Estimation for Earth System Science Applications”. In: *Artificial Intelligence for the Earth Systems 3.4* (Oct. 2024). arXiv:2309.13207 [cs], p. 230093. ISSN: 2769-7525. DOI: [10.1175/AIES-D-23-0093.1](https://doi.org/10.1175/AIES-D-23-0093.1). URL: <http://arxiv.org/abs/2309.13207> (visited on 01/04/2026).
- [13] P. Spirtes, C. Glymour, and R. Scheines. “Causation, Prediction, and Search, 2nd Edition”. In: 2001. URL: <https://www.semanticscholar.org/paper/Causation%2C-Prediction%2C-and-Search%2C-2nd-Edition-Spirtes-Glymour/22260d24042bf9661196a0817e3102f1092bed86> (visited on 01/24/2026).
- [14] David Maxwell Chickering. “Optimal structure identification with greedy search”. In: *J. Mach. Learn. Res.* 3.null (Mar. 2003), pp. 507–554. ISSN: 1532-4435. DOI: [10.1162/153244303321897717](https://doi.org/10.1162/153244303321897717). URL: <https://dl.acm.org/doi/10.1162/153244303321897717> (visited on 01/24/2026).
- [15] Akim Kotelnikov et al. *TabDDPM: Modelling Tabular Data with Diffusion Models*. arXiv:2209.15421 [cs]. Oct. 2024. DOI: [10.5555/3618408.3619133](https://doi.org/10.5555/3618408.3619133). URL: <http://arxiv.org/abs/2209.15421> (visited on 01/04/2026).
- [16] Nick Pawlowski, Daniel C. Castro, and Ben Glocker. *Deep Structural Causal Models for Tractable Counterfactual Inference*. arXiv:2006.06485 [stat]. Oct. 2020. DOI: [10.48550/arXiv.2006.06485](https://doi.org/10.48550/arXiv.2006.06485). URL: <http://arxiv.org/abs/2006.06485> (visited on 01/04/2026).
- [17] Patrick Chao et al. *Modeling Causal Mechanisms with Diffusion Models for Interventional and Counterfactual Queries*. arXiv:2302.00860 [stat]. Oct. 2024. DOI: [10.48550/arXiv.2302.00860](https://doi.org/10.48550/arXiv.2302.00860). URL: <http://arxiv.org/abs/2302.00860> (visited on 01/04/2026).
- [18] Ilyes Khemakhem et al. *Causal Autoregressive Flows*. arXiv:2011.02268 [stat]. Feb. 2021. DOI: [10.48550/arXiv.2011.02268](https://doi.org/10.48550/arXiv.2011.02268). URL: <http://arxiv.org/abs/2011.02268> (visited on 01/04/2026).

- [19] Murat Kocaoglu et al. *CausalGAN: Learning Causal Implicit Generative Models with Adversarial Training*. arXiv:1709.02023 [cs]. Sept. 2017. DOI: [10 . 48550 / arXiv . 1709 . 02023](https://doi.org/10.48550/arXiv.1709.02023). URL: [http : // arxiv . org / abs / 1709 . 02023](http://arxiv.org/abs/1709.02023) (visited on 01/04/2026).
- [20] Zhaozhi Qian, Bogdan-Constantin Cebere, and Mihaela van der Schaar. *Syntheticity: facilitating innovative use cases of synthetic data in different data modalities*. arXiv:2301.07573 [cs]. Jan. 2023. DOI: [10 . 48550 / arXiv . 2301 . 07573](https://doi.org/10.48550/arXiv.2301.07573). URL: [http : // arxiv . org / abs / 2301 . 07573](http://arxiv.org/abs/2301.07573) (visited on 01/04/2026).
- [21] Michael J. McGeachie, Hsun-Hsien Chang, and Scott T. Weiss. “CGBayesNets: Conditional Gaussian Bayesian Network Learning and Inference with Mixed Discrete and Continuous Data”. en. In: *PLOS Computational Biology* 10.6 (June 2014), e1003676. ISSN: 1553-7358. DOI: [10 . 1371 / journal . pcbi . 1003676](https://doi.org/10.1371/journal.pcbi.1003676). URL: [https : // journals . plos . org / ploscompbiol / article ? id = 10 . 1371 / journal . pcbi . 1003676](https://journals.plos.org/ploscompbiol/article?id=10.1371/journal.pcbi.1003676) (visited on 01/04/2026).
- [22] Regis Houssou et al. *Generation and Simulation of Synthetic Datasets with Copulas*. arXiv:2203.17250 [cs]. Mar. 2022. DOI: [10 . 48550 / arXiv . 2203 . 17250](https://doi.org/10.48550/arXiv.2203.17250). URL: [http : // arxiv . org / abs / 2203 . 17250](http://arxiv.org/abs/2203.17250) (visited on 01/04/2026).
- [23] Vikram Mullachery, Aniruddh Khera, and Amir Husain. *Bayesian Neural Networks*. arXiv:1801.07710 [cs]. Jan. 2018. DOI: [10 . 48550 / arXiv . 1801 . 07710](https://doi.org/10.48550/arXiv.1801.07710). URL: [http : // arxiv . org / abs / 1801 . 07710](http://arxiv.org/abs/1801.07710) (visited on 01/04/2026).
- [24] Gero Walter. “A Technical Note on the Dirichlet-Multinomial Model”. en. In: (2009).
- [25] James Dougherty, Ron Kohavi, and Mehran Sahami. “Supervised and Unsupervised Discretization of Continuous Features”. en-US. In: *Machine Learning Proceedings 1995*. Morgan Kaufmann, Jan. 1995, pp. 194–202. DOI: [10 . 1016 / B978 - 1 - 55860 - 377 - 6 . 50032 - 3](https://doi.org/10.1016/B978-1-55860-377-6.50032-3). URL: [https : // www . sciencedirect . com / science / chapter / edited - volume / abs / pii / B9781558603776500323](https://www.sciencedirect.com/science/chapter/edited-volume/abs/pii/B9781558603776500323) (visited on 01/04/2026).
- [26] Balaji Lakshminarayanan. “Decision Trees and Forests: A Probabilistic Perspective”. en. In: (2016).
- [27] Yaojun Zhang et al. *Bayesian CART models for aggregate claim modeling*. arXiv:2409.01908 [stat]. Aug. 2025. DOI: [10 . 48550 / arXiv . 2409 . 01908](https://doi.org/10.48550/arXiv.2409.01908). URL: [http : // arxiv . org / abs / 2409 . 01908](http://arxiv.org/abs/2409.01908) (visited on 01/04/2026).
- [28] Eyke Hüllermeier and Willem Waegeman. “Aleatoric and Epistemic Uncertainty in Machine Learning: An Introduction to Concepts and Methods”. In: *Machine Learning* 110.3 (Mar. 2021). arXiv:1910.09457 [cs], pp. 457–506. ISSN: 0885-6125, 1573-0565. DOI: [10 . 1007 / s10994 - 021 - 05946 - 3](https://doi.org/10.1007/s10994-021-05946-3). URL: [http : // arxiv . org / abs / 1910 . 09457](http://arxiv.org/abs/1910.09457) (visited on 01/21/2026).
- [29] Yarin Gal. “Uncertainty in Deep Learning”. PhD thesis. University of Cambridge, 2016. URL: [https : // www . cs . ox . ac . uk / people / yarin . gal / website / thesis / thesis . pdf](https://www.cs.ox.ac.uk/people/yarin.gal/website/thesis/thesis.pdf).
- [30] Burcu Can and Suresh Manandhar. “Tree Structured Dirichlet Processes for Hierarchical Morphological Segmentation”. In: *Computational Linguistics* 44.2 (June 2018). Place: Cambridge, MA, pp. 349–374. DOI: [10 . 1162 / COLI _ a _ 00318](https://doi.org/10.1162/COLI_a_00318). URL: [https : // aclanthology . org / J18 - 2005 /](https://aclanthology.org/J18-2005/) (visited on 01/04/2026).
- [31] John Salvatier, Thomas Wiecki, and Christopher Fonnesbeck. *Probabilistic Programming in Python using PyMC*. arXiv:1507.08050 [stat]. July 2015. DOI: [10 . 48550 / arXiv . 1507 . 08050](https://doi.org/10.48550/arXiv.1507.08050). URL: [http : // arxiv . org / abs / 1507 . 08050](http://arxiv.org/abs/1507.08050) (visited on 01/10/2026).
- [32] Patrik Hoyer et al. “Nonlinear causal discovery with additive noise models”. In: *Advances in Neural Information Processing Systems*. Vol. 21. Curran Associates, Inc., 2008. URL: [https : // papers . nips . cc / paper / 2008 / hash / f7664060cc52bc6f3d620bcedc94a4b6 - Abstract . html](https://papers.nips.cc/paper/2008/hash/f7664060cc52bc6f3d620bcedc94a4b6-Abstract.html) (visited on 01/09/2026).
- [33] Pearl Judea. *Causality: Models, Reasoning, and Inference*. 2nd ed. Cambridge University Press, 2009. ISBN: 978-0-521-89560-6.
- [34] Pedro Sanchez and Sotirios A. Tsaftaris. *Diffusion Causal Models for Counterfactual Estimation*. arXiv:2202.10166 [cs]. Feb. 2022. DOI: [10 . 48550 / arXiv . 2202 . 10166](https://doi.org/10.48550/arXiv.2202.10166). URL: [http : // arxiv . org / abs / 2202 . 10166](http://arxiv.org/abs/2202.10166) (visited on 01/04/2026).
- [35] Pablo Sanchez-Martin, Miriam Rateike, and Isabel Valera. *VACA: Design of Variational Graph Autoencoders for Interventional and Counterfactual Queries*. arXiv:2110.14690 [stat]. Oct. 2021. DOI: [10 . 48550 / arXiv . 2110 . 14690](https://doi.org/10.48550/arXiv.2110.14690). URL: [http : // arxiv . org / abs / 2110 . 14690](http://arxiv.org/abs/2110.14690) (visited on 01/04/2026).
- [36] Arthur Gretton et al. *A Kernel Method for the Two-Sample Problem*. arXiv:0805.2368 [cs]. May 2008. DOI: [10 . 48550 / arXiv . 0805 . 2368](https://doi.org/10.48550/arXiv.0805.2368). URL: [http : // arxiv . org / abs / 0805 . 2368](http://arxiv.org/abs/0805.2368) (visited on 01/04/2026).

- [37] Joymallya Chakraborty, Suvodeep Majumder, and Tim Menzies. “Bias in Machine Learning Software: Why? How? What to do?” In: *Proceedings of the 29th ACM Joint Meeting on European Software Engineering Conference and Symposium on the Foundations of Software Engineering*. arXiv:2105.12195 [cs]. Aug. 2021, pp. 429–440. DOI: [10 . 1145 / 3468264 . 3468537](https://doi.org/10.1145/3468264.3468537). URL: <http://arxiv.org/abs/2105.12195> (visited on 01/04/2026).
- [38] Alekh Agarwal et al. *A Reductions Approach to Fair Classification*. arXiv:1803.02453 [cs]. July 2018. DOI: [10 . 48550 / arXiv . 1803 . 02453](https://doi.org/10.48550/arXiv.1803.02453). URL: <http://arxiv.org/abs/1803.02453> (visited on 01/04/2026).
- [39] Moritz Hardt, Eric Price, and Nathan Srebro. *Equality of Opportunity in Supervised Learning*. arXiv:1610.02413 [cs]. Oct. 2016. DOI: [10 . 48550 / arXiv . 1610 . 02413](https://doi.org/10.48550/arXiv.1610.02413). URL: <http://arxiv.org/abs/1610.02413> (visited on 01/04/2026).
- [40] Cynthia Dwork et al. *Fairness Through Awareness*. arXiv:1104.3913 [cs]. Nov. 2011. DOI: [10 . 48550 / arXiv . 1104 . 3913](https://doi.org/10.48550/arXiv.1104.3913). URL: <http://arxiv.org/abs/1104.3913> (visited on 01/04/2026).
- [41] Matt J. Kusner et al. *Counterfactual Fairness*. arXiv:1703.06856 [stat]. Mar. 2018. DOI: [10 . 48550 / arXiv . 1703 . 06856](https://doi.org/10.48550/arXiv.1703.06856). URL: <http://arxiv.org/abs/1703.06856> (visited on 01/04/2026).
- [42] Xun Zheng et al. *DAGs with NO TEARS: Continuous Optimization for Structure Learning*. arXiv:1803.01422 [stat]. Nov. 2018. DOI: [10 . 48550 / arXiv . 1803 . 01422](https://doi.org/10.48550/arXiv.1803.01422). URL: <http://arxiv.org/abs/1803.01422> (visited on 01/04/2026).
- [43] Larissa N. A. Martins, Flávio B. Gonçalves, and Thais P. Galletti. *Generation and analysis of synthetic data via Bayesian networks: a robust approach for uncertainty quantification via Bayesian paradigm*. arXiv:2402.17915 [stat]. Mar. 2024. DOI: [10 . 48550 / arXiv . 2402 . 17915](https://doi.org/10.48550/arXiv.2402.17915). URL: <http://arxiv.org/abs/2402.17915> (visited on 01/04/2026).
- [44] Muhammad Aitsam. “Differential Privacy Made Easy”. In: *2022 International Conference on Emerging Trends in Electrical, Control, and Telecommunication Engineering (ETEECTE)*. arXiv:2201.00099 [cs]. Dec. 2022, pp. 1–7. DOI: [10 . 1109 / ETEECTE55893 . 2022 . 10007322](https://doi.org/10.1109/ETEECTE55893.2022.10007322). URL: <http://arxiv.org/abs/2201.00099> (visited on 01/04/2026).
- [45] Ashwin Machanavajjhala et al. “L-diversity: Privacy beyond k-anonymity”. In: *ACM Trans. Knowl. Discov. Data* 1.1 (Mar. 2007), 3–es. ISSN: 1556-4681. DOI: [10 . 1145 / 1217299 . 1217302](https://doi.org/10.1145/1217299.1217302). URL: <https://doi.org/10.1145/1217299.1217302> (visited on 01/04/2026).